Topographic Normalization of TM Scenes through the Use of an Atmospheric Correction Method and Digital Terrain Models

Abstract

The correction for the topographic effect of remotely sensed images taken over rugged terrains has been dealt with by various procedures. The calculation of some crucial atmospheric parameters is needed to normalize deterministically the spectral responses of differently oriented slopes. In a previous model, the authors estimated beam transmittance and diffuse light for TM scenes by using easily attainable information so as to compute surface reflectances. On the basis of this knowledge and of a Lambertian assumption, a procedure has been developed which uses digital terrain models to normalize topographically the spectral responses of rugged areas. The procedure was tested in a case study in Tuscany using TM scenes from three seasons. The results, estimated both visually and statistically, show the potential of the method along with some limitations which are critically discussed.

Introduction

The use of remotely sensed data in highly rugged terrain has often been accompanied by major difficulties because of variations in illumination and reflection geometry caused by different slope angles and orientations. The images acquired by high resolution sensors such as the Landsat Thematic Mapper (TM) and the SPOT HRV are particularly affected by this problem, which results in darker slopes facing away from the sun and brighter sun-facing slopes.

Various methods have been proposed to correct remotely sensed images for the topographic effect. A simple strategy consists in the statistical transformation of the original images to reduce the effect: band ratios (Holben and Justice, 1981) Principal Component (Conese *et al.*, 1988; 1993), and Hiperpherical Direction Cosine (Pouch and Campagna, 1990) transformations have been used in this context. Even though these methods have yielded good results, they generally imply a loss in statistical information and precision.

A more general strategy is represented by the use of digital terrain models (DTM) to take into account the topography of the area. In this case, one of the first results achieved was that a simple normalization based on a cosine law of the light incident angle was usually not effective, resulting in overcorrections (Civco, 1989; Colby, 1991). This behavior was mainly attributed to the inadequacy of the Lambertian assumption, but could be due also to the lack of consideration of the diffuse component of light. In several approaches, empirical coefficients were utilized, estimated statistically for each image, and were variable for each spectral band (Civco, 1989; Colby, 1991; Naugle and Lashlee, 1992). Being scene dependent, these coefficients must be determined for each unique set of solar-terrain geometries and image content, which is a major limitation of most statistical methods.

On the other hand, in order to correct for the topographic effect in a deterministic way, knowledge of the atmospheric condition at the time of the satellite overpass is needed, because this determines the transmittance of direct radiation and the amount of diffuse light. The difficulty in achieving this knowledge, especially in retrospective studies, has prevented a more straightforward solution of the problem. In effect, a method for the topographic normalization of remotely sensed scenes could find its maximum efficiency only when inserted into a general model of atmospheric correction for estimating the real reflectances of the surfaces examined.

An atmospheric correction model for retrieving surface reflectances from TM images was presented by the authors in a recent investigation (Gilabert *et al.*, 1992). A peculiar feature of the procedure was that it requires only easily attainable inputs and the identification of some dark points in TM bands 1 and 3. From this information, an approximate knowledge of the atmospheric condition can be obtained, so that surface reflectances can be computed for almost all the TM scenes generally employed. In the model, the atmospheric beam transmittance and the diffuse irradiance are estimated, which are the critical parameters to compute the total irradiance on a point when its position is known (Proy *et al.*, 1991). Thus, the method can be extended to compute, with the aid of a DTM, the irradiance on each pixel of a TM scene taken over rugged terrain. Consequently, a straightforward computation of the hemispherical surface reflectance can be made relying on a Lambertian assumption.

In the present paper, after a concise presentation of the atmospheric correction method, the procedure for calculating the incident light and, consequently, the surface reflectance of each TM pixel on the basis of a DTM, is presented. Then, the methodology is applied to a study site with rugged ter-

Photogrammetric Engineering & Remote Sensing,
Vol. 59, No. 12, December 1993, pp. 1745–1753.

0099-1112/93/5912–1745$03.00/0

C. Conese
I.A.T.A.-C.N.R., P. le delle Cascine 18, 50144 Firenze, Italy.
M. A. Gilabert
Departament de Termodinàmica, Facultat de Fisica,
Universitat de València, 46100-Burjassot, València, Spain.
F. Maselli
L. Bottai
I.A.T.A.-C.N.R., P. le delle Cascine 18, 50144 Firenze, Italy.

rain in central Italy for which three TM acquisitions from different seasons (winter, spring, and summer, 1988) were available. Topographically corrected reflectance images were obtained and compared to those not topographically corrected. Because some ground references under different illumination conditions were present in the study area, a statistical analysis was also undertaken to test for the significance of the reflectance differences between shadowed and illuminated pixels before and after the topographic correction. Finally, an advanced classification procedure was applied to the uncorrected and corrected scenes; the different performances of the classifier due to the different illumination conditions were evaluated by means of Kappa coefficients of agreement.

Atmospheric Correction Model

The method proposed by the authors (Gilabert *et al.*, 1992) consists of an inversion technique based on a simplified radiative transfer model in the atmosphere. A horizontally homogeneous atmosphere is assumed, so that transmittance and path radiance are constant over the scene and their value can be determined for each image. On the basis of the presence of dark points (reflectance approximately zero) in the imaged scenes and using a combination of two TM bands (TM1 and TM3) the actual aerosol model is estimated through the wavelength dependence of the aerosol path radiance. In this way, an approximated knowledge of the atmosphere composition and structure is possible, and the retrieval of actual reflectances from the sensed images can be carried out. Assuming that the Earth's surface is Lambertian, these reflectances, $R_S(\lambda)$, as measured from satellite, can be approximated by the expression

$$R_S(\lambda) = [k\pi L_S(\lambda)]/[E_g(\lambda)\cos\theta_0] \quad (1)$$

where

$R_S(\lambda)$ is the reflectance of the surface at wavelength λ (dimensionless);
$L_S(\lambda)$ is the radiance of the surface, that is, the radiance of light transmitted downward through the atmosphere and reflected on the surface ($Wm^{-2}\mu m^{-1}sr^{-1}$);
$E_g(\lambda)$ is the global solar irradiance ($Wm^{-2}\mu m^{-1}$) on the horizontal surface;
θ_0 is the solar zenith angle; and
k is a factor (dimensionless) which accounts for the change in the sun-Earth distance.

The atmospheric effect is taken into account to compute the reflectance through the terms $L_S(\lambda)$ and $E_g(\lambda)$ of Equation 1.

Surface radiance, $L_S(\lambda)$, is computed by using the expression

$$L_S(\lambda) = [L_0(\lambda) - L_p(\lambda)]/T(\lambda,\theta) \quad (2)$$

where

$L_0(\lambda)$ is the remotely sensed radiance (sensor calibration);
$L_p(\lambda)$ is the path radiance (contribution from the scattering of the direct sun beam by the atmospheric constituents), computed using the dark values found in the image; and
$T(\lambda,\theta)$ is the beam transmittance of the atmosphere in the upward direction, which, for vertical observation, can be approximated by the expression

$$T(\lambda,\theta) = \exp(-\tau_{oz} - \tau_r - \tau_a) \quad (3)$$

where

τ_{oz} is the ozone optical thickness (Sturm, 1981);
τ_r the molecular optical thickness (Kaufman, 1989; Zibordi and Maracci, 1988); and
τ_a is the aerosol optical thickness.

According to the model proposed, the aerosol optical thickness is approximated by

$$\tau_a \approx [4\pi L_a(\lambda,\theta_0)]/[P'_a(\theta_0)w_0] \quad (4)$$

where

L_a is the aerosol contribution to the path radiance, which can be computed using the global path radiance (from the dark pixels in the image) and the molecular path radiance (Saunders, 1990); and
P'_a is a new aerosol phase function defined in the model as

$$P'_a(\theta_0) = \text{PER}^*P_r(\theta_0) + (1 - \text{PER})^*P_a(\theta_0). \quad (5)$$

In this equation $P_a(\theta_0)$ is the aerosol phase function, which can be approximated by the Two-Term Henyey-Grenstein (TTHG) phase function (Aranuvachapun, 1983; Liou, 1980), $P_r(\theta_0)$ is the Rayleigh phase function, and PER is a "percentage of molecular atmosphere" which has been introduced to take into account the "kind of atmosphere" through the wavelength dependence of L_a (Chavez, 1989). Thus, PER=1 would correspond to an ideal Rayleigh atmosphere with non-absorbing aerosols, and PER=0 would correspond to a hazy atmosphere with a higher proportion of absorbing aerosols in a typical agricultural environment (Iqbal, 1983). The aforementioned dependence has been determined using the dark values in bands TM1 and TM3.

w_0 is the aerosol single scattering albedo, computed in the model using

$$w_0 = \text{PER}^*1.00 + (1 - \text{PER})^*0.90 \quad (6)$$

where 1.00 and 0.90 are the values of the aerosol single scattering albedos which correspond, respectively, to the two kinds of atmosphere described above (i.e., Rayleigh and hazy).

Global solar irradiance on a horizontal surface, $E_g(\lambda)$, can be obtained as the sum of direct (beam) irradiance and diffuse irradiance: i.e.,

$$E_g(\lambda) = E_b(\lambda) + E_d(\lambda) \quad (7)$$

where g refers to global, b to direct (beam), and d to diffuse irradiances.

The expression for direct irradiance is

$$E_b(\lambda) = E_0(\lambda)\cos\theta_0 T(\lambda,\theta_0) \quad (8)$$

where

$E_0(\lambda)$ is the extraterrestrial solar irradiance (Price, 1987); and
$T(\lambda,\theta_0)$ is the beam transmittance in the downward direction, given by

$$T(\lambda,\theta_0) = \exp\{(-\tau_{oz} - \tau_r - \tau_a)/\cos\theta_0\}. \quad (9)$$

If the diffuse irradiance due to multiple reflections between the ground and the atmosphere is neglected, the diffuse irradiance can be approximated by the expression

$$Ed(\lambda) = (1/2)E_0\cos\theta_0[1 - t_r(\lambda,\theta_0)]t_a(\lambda,\theta_0)t_{oz}(\lambda,\theta_0) + F_c(\theta_0)E_0\cos\theta_0[1 - t_a(\lambda,\theta_0)]t_r(\lambda,\theta_0)t_{oz}(\lambda,\theta_0)w_0 \quad (10)$$

where

$$t_r(\lambda,\theta_0) = \exp\{-\tau_r/\cos\theta_0\}, \quad (11)$$

$$t_a(\lambda,\theta_0) = \exp\{-\tau_a/\cos\theta_0\}, \text{ and} \quad (12)$$

$$t_{oz}(\lambda,\theta_0) = \exp\{-\tau_{oz}/\cos\theta_0\}. \quad (13)$$

Equation 10 takes into account the isotropic nature of the Rayleigh scattering by means of the factor (1/2), and the non-isotropic nature of the aerosol scattering by means of the factor $F_c(\theta_0)$ (Iqbal, 1983).

Present Algorithm for Topographic Normalization

Neglecting the multiple reflections between the ground and the atmosphere, the global irradiance on a horizontal surface is independent of the ground reflectance and can be considered as an intrinsic atmospheric function, with a given value for the entire scene (where the atmosphere is assumed homogeneous), as can be seen in Equations 7 to 13.

In mountainous terrain, even under the assumption of a homogeneous atmosphere, global irradiance must be calculated for each pixel of the image, because there is another factor to be taken into account; the Sun-target orientation-sensor geometry, which can vary from one pixel to another. For this reason, equations 8 and 10 must be modified to take into account the topographic effect, which mainly affects global irradiance in two ways (Proy *et al.*, 1989): (1) direct and diffuse irradiances may vary according to the angle β, formed by the solar beam and the normal to the surface; and (2) topographic irregularities can cast shadows on a pixel so that it does not receive direct radiation.

The modeling of solar radiation on non-horizontal surfaces is more complex than the modeling for horizontal surfaces, due to the effect of configuration factors and to diffuse anisotropy over the sky dome. In recent years a number of models have been proposed to estimate solar radiation on tilted surfaces (Iqbal, 1983; Utrillas *et al.*, 1991). The main differences between most approaches are in the modeling of the sky-diffuse irradiance.

If the symbol (*) is used to indicate the magnitudes referred to a non-horizontal surface, the expression for the beam irradiance term is given by

$$E_b^*(\lambda) = E_0(\lambda)\cos\beta T(\lambda,\theta_0) \quad \text{if} \quad \cos\beta > 0 \quad (14)$$

$$E_b^*(\lambda) = 0 \quad \text{if} \quad \cos\beta < 0 \quad (15)$$

where β is the angle between the solar rays and the normal to the surface.

As can be seen, Equation 15 accounts for the case of those pixels which are completely in shadow and do not receive direct solar radiation.

The first models for diffuse irradiance on a tilted surface assumed an isotropic distribution of diffuse solar radiation over the sky dome (Iqbal, 1983). In this way, the diffuse solar radiation on a tilted plane is given by the diffuse solar radiation on a horizontal plane corrected by a geometrical configuration factor. Temps and Coulson (1977) showed that diffuse radiation is anisotropic over the sky dome, increasing in the near horizon and in the circumsolar zone. They proposed some correction factors for these two zones.

In this paper, Hay's model will be used (Hay, 1979; Hay and McKay, 1985; Hay *et al.*, 1986), which takes into account an anisotropic distribution of diffuse radiation. This model considers two different contributions to diffuse irradiance: a circumsolar one for the near-the-sun sky-dome and an isotropic-distributed one for the rest of the sky-dome. Their relative weight depends on the anisotropy index (E_b/E_0), which is shown in Table 1 for all the scenes used. Hay assumes linearity on the isotropic and circumsolar contribution to diffuse radiation on a tilted plane. Therefore, this is given by

$$E_d^* = E_d\{[E_b/E_0][\cos\beta/\cos\theta_0] + (1/2)[1 - (E_b/E_0)][1 + \cos\theta_n]\} \quad (16)$$

where θ_n is the slope of the terrain (zenith angle of the normal to the surface).

The new value for global irradiance will be

$$E_g^*(\lambda) = E_b^*(\lambda) + E_d^*(\lambda) \quad (17)$$

which should be used in Equation 1 instead of $E_g(\lambda)$ to account for the topographic effect. As can be seen, the correction now will be different for each pixel because of the angles β and θ_n, which have different values according to the pixel location. These two angles are provided by the digital terrain model.

Case Study

Study Area and Satellite Data

A rural area south of Florence, Italy (43°40′ north latitude, 11° 10′ east longitude) was chosen as the test site. Four zones, each approximately 10 by 10 km in size, were considered. They corresponded to four I.G.M. (Istituto Geografico Militare) 1:25,000-scale topographic maps in the area known as "Chianti." As fully described in Conese and Maselli (1991), this zone has a typical Mediterranean climate and is gently rugged, with elevations that range between 200 and 900 m and maximum slopes of approximately 25 percent. The area is covered mainly by mixed deciduous and coniferous forests, olive groves, and vineyards.

From an accurate ground survey and interpretation of aerial photographs, seven cover types were deemed sufficient to characterize the land use of the area (Table 2). The ground references were collected during summer and fall of 1988 using a stratified random sampling design. Many small plots were identified in the study area, each corresponding to a quite homogeneous surface of about 1 ha.

Thematic Mapper (TM) data were obtained from three Landsat 5 overpasses taken during different seasons: 20 February 1988 (acquisition A), 25 May 1988 (acquisition B), and 14 August 1988 (acquisition C). These three dates of TM data allowed the use of images with different sun zenith angles, so as to consider quite different illumination conditions. Four subscenes for each date were extracted from TM frame

TABLE 1. MAIN CHARACTERISTICS OF THE TM SCENES USED IN THE STUDY: DATE, SOLAR ZENITH ANGLE (θ_0), AND ANISTROPY INDEX OF THE HAY'S MODEL TO DETERMINE THE DIFFUSE IRRADIANCE ON NON-HORIZONTAL SURFACES.

Scene	Date	θ_0 (°)	Anistropy Index (E_b/E_0)
A	20 February	64.7	TM1 → 0.24 TM2 → 0.29 TM3 → 0.34 TM4 → 0.39 TM5 → 0.42 TM7 → 0.43
B	26 May	38.3	TM1 → 0.57 TM2 → 0.62 TM3 → 0.67 TM4 → 0.72 TM5 → 0.77 TM7 → 0.77
C	14 August	43.7	TM1 → 0.45 TM2 → 0.50 TM3 → 0.55 TM4 → 0.60 TM5 → 0.66 TM7 → 0.67

TABLE 2. COVER TYPES OF THE STUDY AREA WITH THE NUMBER OF REFERENCE PLOTS.

Class	Cover Type	Number of Reference Plots
1	Pine forest	39
2	Chestnut forest	23
3	Oak forest (i)	49
4	Oak forest (ii)	21
5	Vineyard	36
6	Olive grove	34
7	Urban area	17

192/30, quarter II. The subscenes were georeferenced with respect to the four topographic maps by using a bilinear interpolation algorithm trained on ground control points. At least 10 to 12 points were accurately identified for each map and TM subscene, with resulting RMSEs always less than 1 pixel.

Materials and Methods

Creation of DTMs

The Geosys software package was used for the creation of the DTMs (Geosystems, 1990). This package employes a linear interpolation algorithm for generating DTMs from contour lines. The accuracy of the models obtained obviously depends on the quality and spacing of the contour lines digitized. In the current case, the contour lines were spaced at 25 m and were quite spatially accurate. The acquisition process was accomplished with extreme care by an operator working on a digitizer table. Thus, a maximum accuracy of the output models could be assumed with respect to the maps and algorithm used (Geosystems, 1990). For each map, digital models reporting elevations, slopes, and aspects were generated. From the last two models, and knowing the sun astronomic coordinates at the time of the three satellite passages, a fourth digital model with insolation angles was generated for each study subscene by the formula

$$\beta = \arccos\{\cos\theta_0\cos\theta_n + \sin\theta_0\sin\theta_n\cos(\phi_0 - \phi_n)\} \quad (18)$$

where θ_0 is the solar zenith angle, θ_n is the slope of the terrain, and ϕ_0 and ϕ_n are the solar azimuth angle and the topographic aspect angle, respectively.

Plate 1 shows an example of DTM outputs for a subscene of the acquisition A: (a) shows the altitude of each pixel, and (b) the complement of the insolation angle.

On the basis of the solar zenith angles at Landsat-5 overpass time (see Table 1), the study areas were then divided into illuminated and shadowed pixels by considering, in the three acquisitions, half of the pixels with lower β as sun-facing slopes and the other half as shadowed areas.

Computation of Reflectances

The reflectance values for each TM scene were first calculated by the algorithm of Gilabert *et al.* (1992). Next, using the DTMs, new images were generated according to the equations of the previous two sections. The two series of images (topographically uncorrected and corrected) were then visually examined; an example of color composites is shown in Plate 2.

Extraction of Spectral Signatures and Statistical Analysis

The reference samples were digitized as plots of 3 by 3 TM pixels (90 by 90 m). The seven cover types considered were quite stable during a growing season, so that no spatial variation was assumed for the multitemporal data set. The spectral signatures of the six vegetated cover types in shadowed and illuminated slopes were computed from both the topographically uncorrected and corrected reflectance images. Class 7 (urban area) was not considered because the relevant pixels were almost all located in flat zones. To avoid problems of spatial autocorrelation, only one pixel for each plot was considered. The relevant mean reflectance values for two of the classes are shown in Figures 1 to 3.

Given the approximate homogeneity in composition within each cover class, a similar uniformity in spectral signature could be expected. Hence, possible reflectance differences between dark and sun-facing slopes could be mainly attributed to the effect of topography. To test for the significance of the differences found, a multivariate analysis of variance was performed on the multispectral data considering for each cover class two levels (shadowed and illuminated) before and after the topographic normalization. The probabilities for variance ratios resulting from the analysis are reported in Tables 3 to 5.

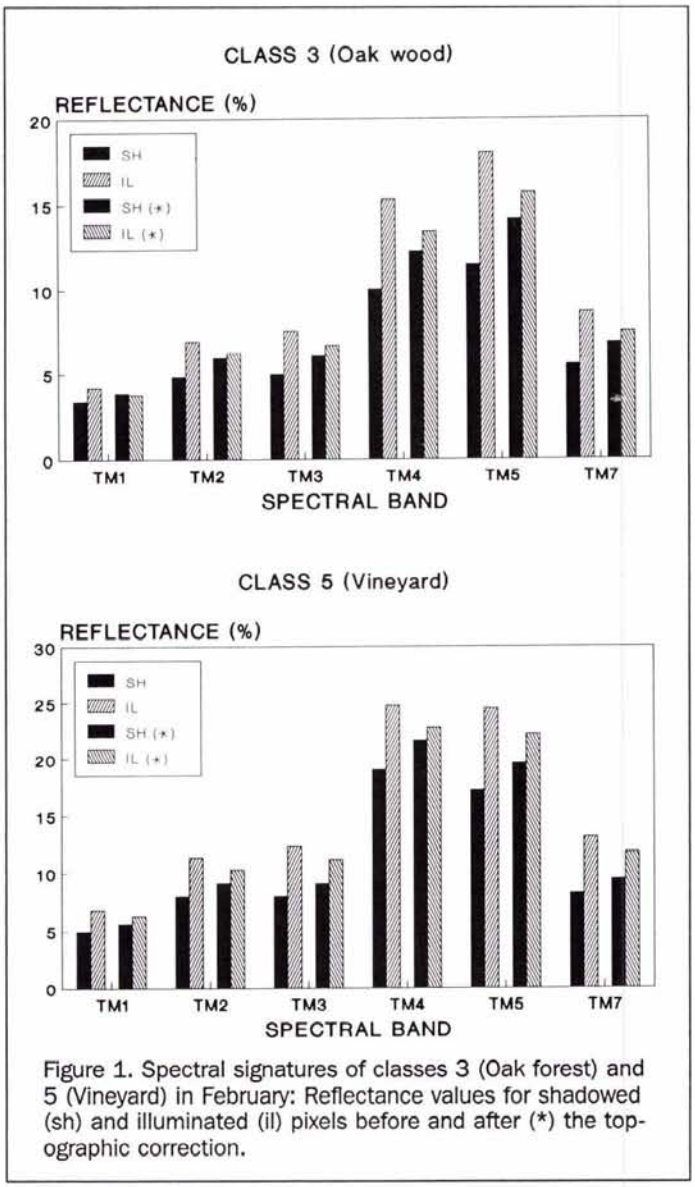

Figure 1. Spectral signatures of classes 3 (Oak forest) and 5 (Vineyard) in February: Reflectance values for shadowed (sh) and illuminated (il) pixels before and after (*) the topographic correction.

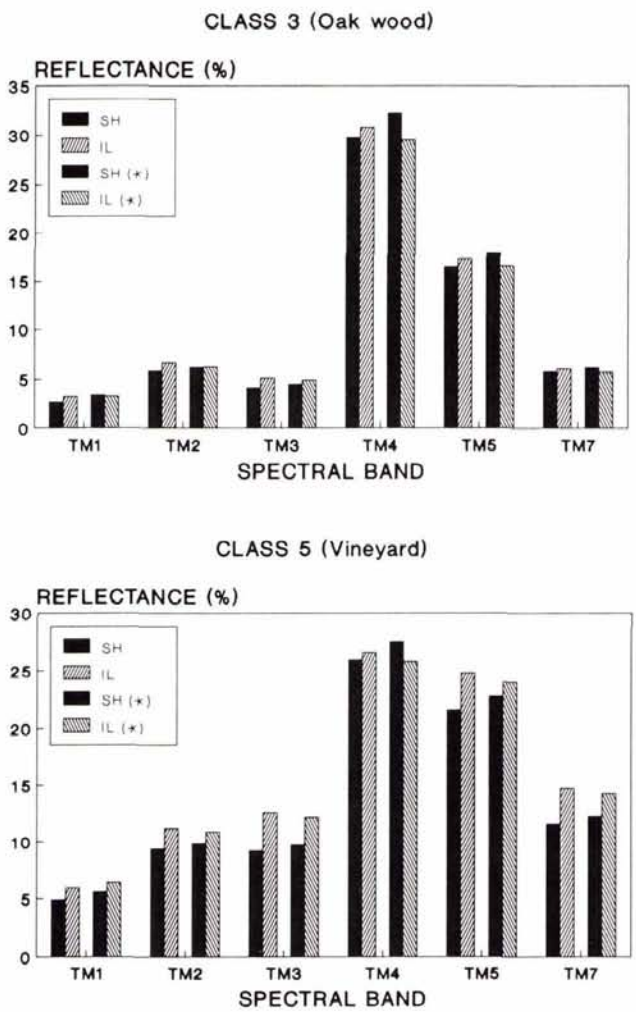

Figure 2. Spectral signatures of classes 3 (Oak forest) and 5 (Vineyard) in May: Reflectance values for shadowed (sh) and illuminated (il) pixels before and after (*) the topographic correction.

Classifications with Uncorrected and Corrected Images

A further quantitative test was made by classifying the uncorrected and corrected images, so as to evaluate the effect of topographic normalization on the statistical discriminability of the seven cover types of the study area. The classification procedure is a modified maximum-likelihood classifier recently proposed by the authors (Maselli *et al.*, 1992), which takes into consideration non-parametric priors. To work properly, the classifier must be applied to highly informative, almost uncorrelated, channels. According to previous findings (Horler and Ahern, 1986), a subset composed of TM bands 3, 4, and 5 was therefore considered for each scene as the most informative for vegetation studies.

The classification procedure is quite efficient and is also insensitive to differences in illumination conditions, provided that the training pixels are uniformly distributed with respect to illumination conditions. In order to simulate a situation in which this requirement was not satisfied, only the reference areas in illuminated zones were taken for training the classification procedures. Classifications were performed separately on each single date (A:February, B:May, and C:August) of the TM data and on the multitemporal data set using the topographically uncorrected and corrected images. In Plate 3 the two multitemporal classifications of the same subscene as in Plates 1 and 2 are reported.

The final discrimination accuracies were evaluated by means of error matrices compared to all the test pixels. Kappa coefficients of agreement were used as the best measure of accuracy (Congalton *et al.* (1983) with erratum in Hudsom and Ramm (1987)). *Z*-values of the differences due to topographic normalization were also computed to test for their significance (Table 6).

Results

Visual Evaluation

From a first visual evaluation, the topographic effect was clearly apparent in the uncorrected scenes, especially in the February acquisition. An example of images evidently af-

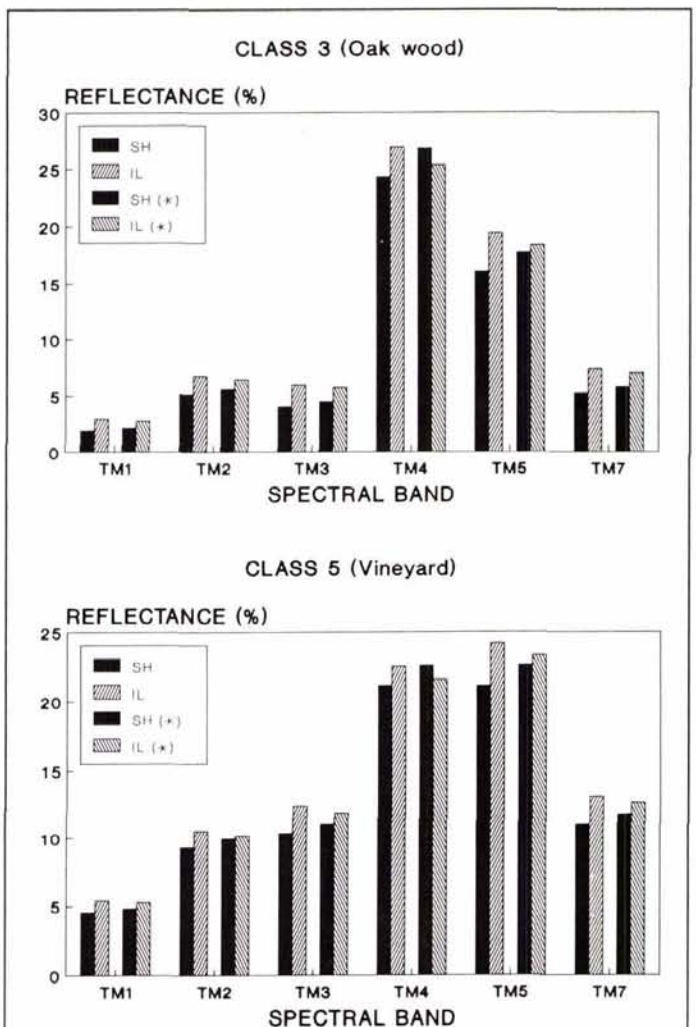

Figure 3. Spectral signatures of classes 3 (Oak forest) and 5 (Vineyard) in August: Reflectance values for shadowed (sh) and illuminated (il) pixels before and after (*) the topographic correction.

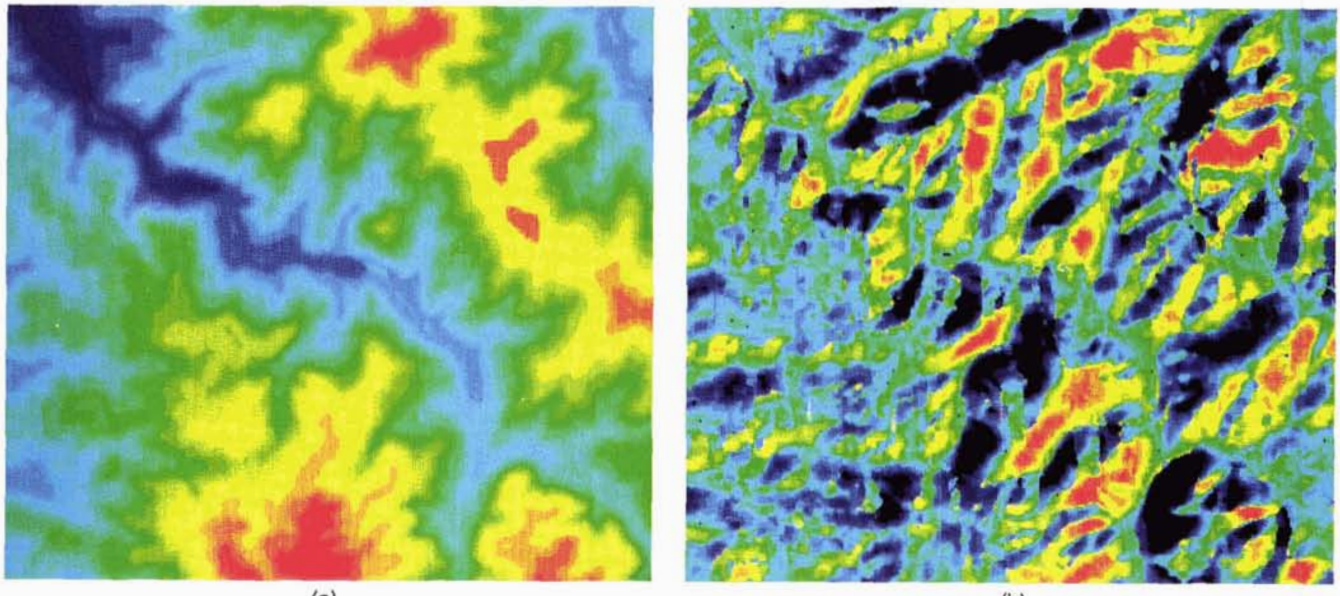

(a) (b)

Plate 1. Outputs of the DTM: (a) altitude and (b) complement of the insolation angle, for a subscene of acquisition A. Color degradation from blue to red indicates increasing values of each magnitude (from 170 to 575 m for (a), and from 100° to 130° for (b)).

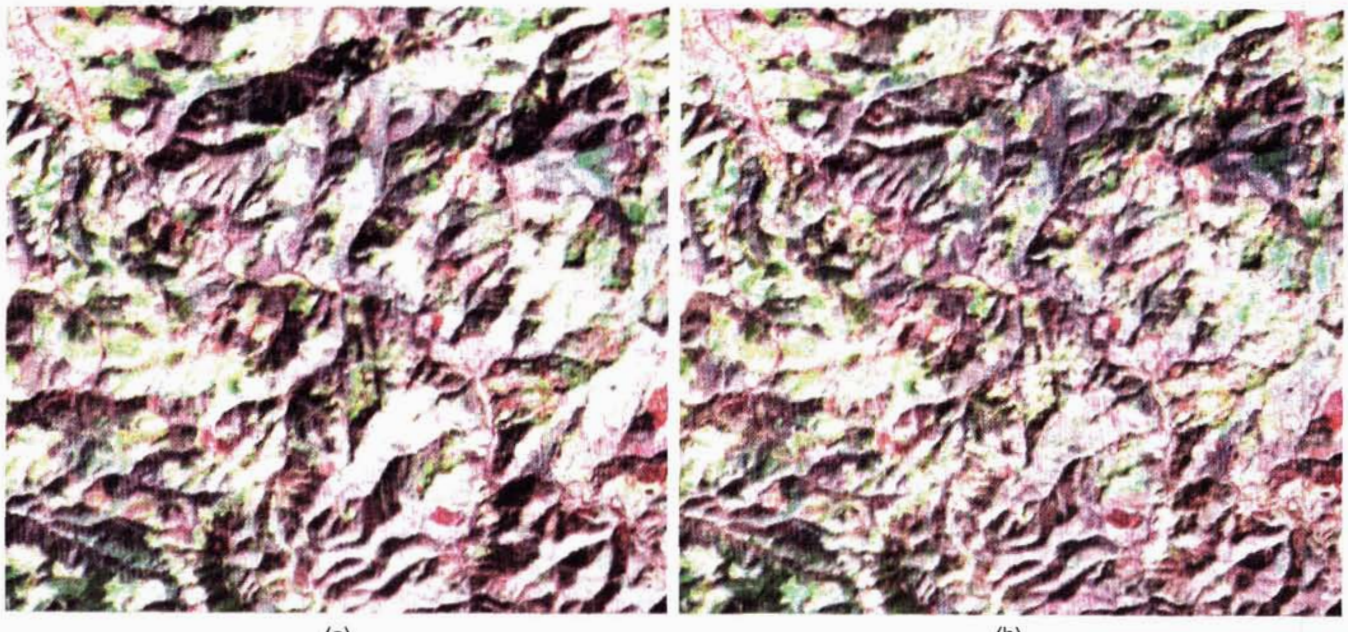

(a) (b)

Plate 2. Color composite (TM3-red, TM4-green, and TM5-blue) of the same subscene as in Plate 1, from acquisition A: (a) with atmospheric correction; (b) with atmospheric and topographic correction.

fected by topography is shown in Plate 2a as a color composite of a winter scene.

The normalization procedure was effective in removing most of the topographic effect. The same subscene as above but normalized is shown in Plate 2b. Most of the topographic irregularities are no longer apparent, although some effects of the topography can be seen in the darkest points. In particular, the correction is evident in the central area of the subscene, while some shadows remain in the lower part, where narrow valleys are present. This persistance of the topo-

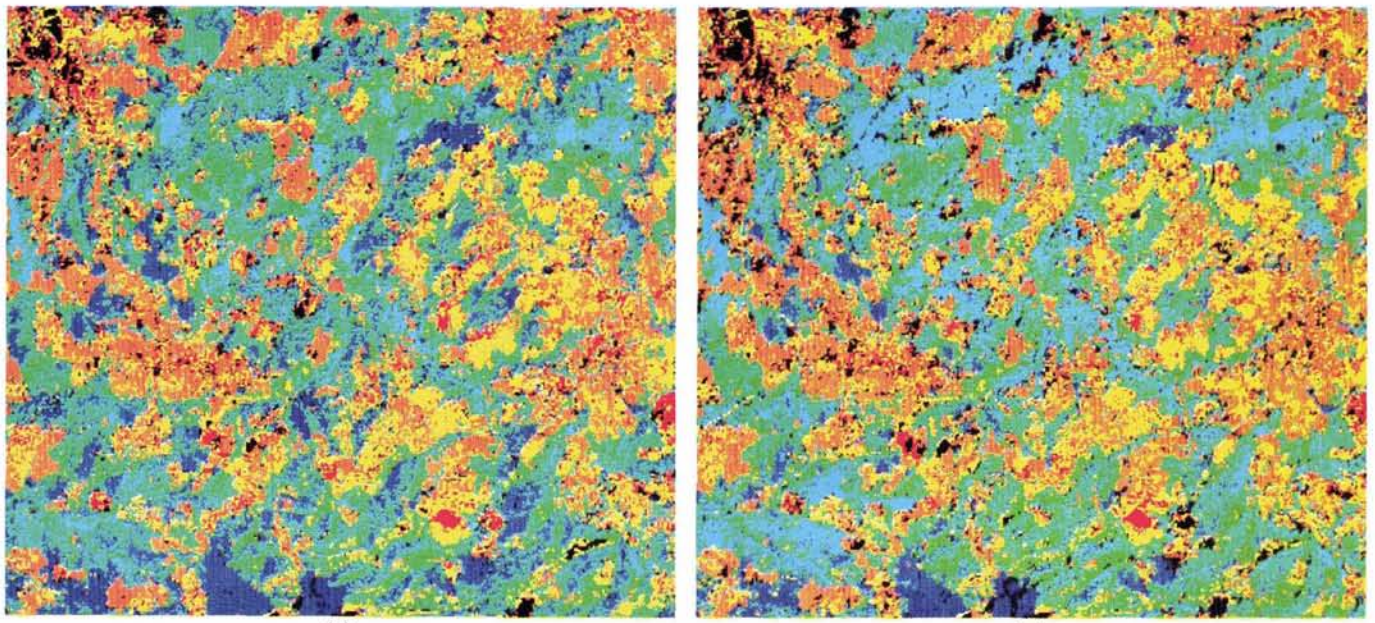

(a) (b)

Plate 3. Classifications of the same subscene as in Plates 1 and 2 obtained with the topographically uncorrected (a) and corrected (b) TM multitemporal data (blue = pine forest, sky blue = chestnut forest, green = oak forest (i), bright green = oak forest (ii), yellow = vineyard, orange = olive grove, red = urban area).

TABLE 3. SCENE A (20 FEBRUARY): PROBABILITIES FOR VARIANCE RATIOS DERIVED FROM THE STATISTICAL ANALYSIS ON SHADOWED AND ILLUMINATED PIXELS. VALUES BEFORE (♦) AND AFTER (♦♦) THE TOPOGRAPHIC CORRECTION ARE GIVEN FOR EACH CLASS IN ALL THE SPECTRAL BANDS.

		Spectral Band					
Class		TM1	TM2	TM3	TM4	TM5	TM7
1	♦	0.07	0.11	0.11	0.04	0.13	0.21
	♦♦	1.00	0.77	0.91	0.53	0.75	0.69
2	♦	<0.01	<0.01	<0.01	<0.01	<0.01	<0.01
	♦♦	0.55	0.80	0.67	0.20	0.06	0.03
3	♦	<0.01	<0.01	<0.01	<0.01	<0.01	<0.01
	♦♦	0.72	0.57	0.37	0.39	0.40	0.48
4	♦	<0.01	<0.01	<0.01	<0.01	<0.01	<0.01
	♦♦	0.22	0.15	0.05	0.02	<0.01	0.02
5	♦	<0.01	<0.01	<0.01	0.03	<0.01	<0.01
	♦♦	0.17	0.12	0.02	0.68	0.14	0.06
6	♦	<0.01	0.03	0.01	0.01	<0.01	<0.01
	♦♦	0.94	0.54	0.63	0.85	0.12	0.50

graphic effect in some zones is common to all the normalized subscenes and will be discussed later; in most cases it can be mainly attributed to the resolution of the DTMs which was not everywhere adequate with respect to that of the TM images.

STATISTICAL ANALYSIS

The examples of spectral signatures reported in Figures 1, 2, and 3 show that the differences between dark and sun-facing slopes are notably reduced by the topographic normalization for all bands.

For the February scene, before normalization, all the

TABLE 4. SCENE B (26 MAY): PROBABILITIES FOR VARIANCE RATIOS DERIVED FROM THE STATISTICAL ANALYSIS ON SHADOWED AND ILLUMINATED PIXELS. VALUES BEFORE (♦) AND AFTER (♦♦) THE TOPOGRAPHIC CORRECTION ARE GIVEN FOR EACH CLASS IN ALL THE SPECTRAL BANDS.

		Spectral Band					
Class		TM1	TM2	TM3	TM4	TM5	TM7
1	♦	0.09	0.04	0.08	0.57	0.09	0.11
	♦♦	0.71	0.73	0.34	0.56	0.49	0.36
2	♦	0.88	0.16	0.97	<0.01	0.01	0.10
	♦♦	0.08	0.54	0.27	0.46	0.50	0.94
3	♦	0.08	0.07	0.06	0.44	0.21	0.52
	♦♦	0.82	0.93	0.42	0.06	0.06	0.31
4	♦	0.53	0.12	0.09	0.04	<0.01	0.05
	♦♦	0.60	0.71	0.45	0.65	0.62	0.36
5	♦	0.05	0.03	<0.01	0.75	0.03	0.04
	♦♦	0.32	0.20	0.05	0.41	0.37	0.18
6	♦	0.92	0.69	0.39	0.05	0.64	0.13
	♦♦	0.34	0.16	0.15	0.73	0.11	0.04

TABLE 5. SCENE C (14 AUGUST): PROBABILITIES FOR VARIANCE RATIOS DERIVED FROM THE STATISTICAL ANALYSIS ON SHADOWED AND ILLUMINATED PIXELS. VALUES BEFORE (♦) AND AFTER (♦ ♦) THE TOPOGRAPHIC CORRECTION ARE GIVEN FOR EACH CLASS IN ALL THE SPECTRAL BANDS.

Class		Spectral Band					
		TM1	TM2	TM3	TM4	TM5	TM7
1	♦	0.21	0.09	0.23	0.61	0.38	0.13
	♦ ♦	0.44	0.36	0.43	0.32	0.97	0.39
2	♦	<0.01	<0.01	<0.01	<0.01	<0.01	<0.01
	♦ ♦	0.34	0.92	0.34	0.59	0.52	0.59
3	♦	0.03	0.03	0.10	0.05	0.01	0.03
	♦ ♦	0.18	0.27	0.29	0.32	0.61	0.20
4	♦	0.08	<0.01	0.05	0.03	<0.01	0.02
	♦ ♦	0.48	0.09	0.19	0.91	0.34	0.22
5	♦	0.12	0.17	0.11	0.26	0.06	0.10
	♦ ♦	0.48	0.82	0.49	0.46	0.68	0.53
6	♦	0.16	0.22	0.27	0.02	0.06	0.14
	♦ ♦	0.48	0.67	0.64	0.97	0.51	0.56

TABLE 6. KAPPA ACCURACIES OF THE CLASSIFICATIONS USING TOPGRAPHICALLY UNCORRECTED (♦) AND CORRECTED (♦ ♦) SCENES, WITH *Z* VALUES OF THE RELEVANT DIFFERENCES (** = HIGHLY SIGNIFICANT).

Scene	Kappa♦	Kappa♦♦	*Z*
A	0.4013	0.4532	2.97(**)
B	0.4262	0.4375	0.64
C	0.4432	0.4983	3.15(**)
ABC	0.5586	0.6161	3.34(**)

ground references located in dark slopes had lower reflectances than those in sun facing slopes. Table 3 shows that these differences were nearly all significant ($P<0.05$) or highly significant ($P<0.01$). The differences were less pronounced and generally non significant for the May scene, clearly due to the higher sun elevation (Table 4). The August scene showed a behavior symilar to that of February, with most marked and significant reflectance differences (Table 5).

In all cases, the normalization process led to an almost complete disappearance of the spectral differences between slopes. The small differences which persisted were generally not significant; a few exceptions, with differences negative or positive in sign, can be probably attributed to reflectance variations within the same class and, above all, to the inaccuracies of the DTMs. The removal of the topographic effect is particularly remarkable for the February scene, where evident shadows were present.

CLASSIFICATIONS

The results of the classifications carried out on the uncorrected and corrected scenes confirmed the findings of the previous statistical analysis. From Plate 3, some differences can be seen in the outcomes of the multitemporal classifications due to the use of uncorrected and corrected data, especially in the central area of the subscene. For instance, a notable decrease in the extent of the pine forest class is apparent with the use of normalized data, probably caused by the reduction of shadowed, dark points which were previously attributed to that category.

The classifications of the uncorrected images resulted in a rather low discrimination accuracy when compared to all the reference pixels (Table 6). In part, this low accuracy can be attributed to the complexity of the cover surfaces examined (Conese and Maselli, 1991). Among the single-date classifications, the scenes of August produced slightly higher accuracies than those of February and May; the multitemporal classification clearly yielded a remarkable improvement.

The use of the normalized images notably increased classification precisions. The improvements obtained in Kappa accuracy were especially notable with the February and August acquisitions, as well as with the multitemporal data set. As seen in Table 6, all these differences were highly significant ($P<0.01$). No significant difference was found for the May acquisition, probably due to the lower sun zenith angle.

Discussion and Conclusions

Topographic normalization of remotely sensed images is a complex problem, which involves several theoretical and practical considerations. The use of a deterministic approach such as that adopted in the present work can find its maximum potential when coupled with a method to compute surface reflectances from satellite imagery. For this, a knowledge of the atmospheric condition at the time of the satellite overpass is needed in order to estimate beam trasmittance and diffuse light. The method of atmospheric correction previously developed by the authors provides this knowledge for TM scenes. Thus, this method, suitably extended as shown in the present paper, allows the computation of the critical parameters for normalizing TM scenes by means of DTMs.

Actually, some drawbacks are inherent in this approach. First, for very dark areas the information contained in the scenes is almost completely lost; thus, even if correctly normalized, these areas cannot provide sufficient information for the discrimination of the cover types. Moreover, the Lambertian assumption, which forms the basis for computing surface reflectances, becomes very weak when the insolation angle falls below a critical value. Consequently, the calculation of reflectances from dark, steep slopes is somewhat unreliable in winter months or for high latitudes.

From the case study examined, another problem arose which is common to most practical applications. Even if the DTMs used were of high quality, their spatial resolution and accuracy was often unsufficient in comparison with that of the TM scenes. In effect, DTMs derived from contour lines acquired every 10 m would be probably necessary for correcting high resolution images. Because maps having these contour lines are rarely available on a regional or sub-regional scale, the topographic normalization of these images is likely to remain rather approximate for some points.

With all these considerations, the results achieved by the use of the method proposed can be judged good, as demonstrated by the statistical analysis. The method is of general and straightforward applicability and can be particularly useful for the correction of TM scenes in retrospective studies, when no ancillary information about the state of the atmosphere and of the surfaces examined is available.

Acknowledgments

The research was partially supported by an ASI (Agenzia Spaziale Italiana) grant. M.A. Gilabert undertook this study at IATA-CNR as a CEAM Research Fellow (Consellería de Cultura, Educació i Ciència de la Generalitat Valenciana, DOGV 15 February 1991). The authors want to thank the *PE&RS* ref-

erees for their useful comments on the first draft of the present paper.

References

Aranuvachapun, S., 1983. Variation of atmospheric optical depth for remote sensing radiance calculations. *Remote Sensing of Environment*, Vol. 13, pp. 131-147.

Chavez, P.S., 1989. Radiometric calibration of Landsat Thematic Mapper multispectral Images. *Photogrammetric Engineering & Remote Sensing*, Vol. 55, No. 9, pp. 1285-1294.

Civco, D.L., 1989. Topographic normalization of Landsat Thematic Mapper digital imagery. *Photogrammetric Engineering & Remote Sensing*, Vol. 55, No. 9, pp. 1303-1309.

Colby, J.D., 1991. Topographic normalization in rugged terrain. *Photogrammetric Engineering & Remote Sensing*, Vol. 57, No. 5, pp. 531-537.

Conese, C., G. Maracchi, F. Miglietta, F. Maselli, and V.M. Sacco, 1988. Forest classification by principal components analyses of TM data. *International Journal of Remote Sensing*, Vol. 9, Nos. 10 and 11, pp. 1597-1612.

Conese, C., G. Maracchi, and F. Maselli, 1993. Improvement in maximum likelihood classification performance on highly rugged terrain using principal component analysis. *International Journal of Remote Sensing*, forthcoming.

Conese, C., and F. Maselli, 1991. Use of multitemporal information to improve classification performance of TM scenes in complex terrain. *ISPRS Journal of Photogrammetry and Remote Sensing*, Vol. 46, pp. 187-197.

Congalton, R.G., R.G. Oderwald, and R.A. Mead, 1983. Assessing Landsat classification accuracy using discrete multivariate analysis statistical techniques. *Photogrammetric Engineering & Re-mote Sensing*, Vol. 49, No. 12, pp. 1671-1678.

Gilabert, M.A., C. Conese, and F. Maselli, 1992. An atmospheric correction method for the automatic retrieval of surface reflectances from TM images. Internal Report, submitted to *International Journal of Remote Sensing*.

Geosystems, 1990. *Software Geosys - Manuali Utente*. Firenze (Italy), March 1990, Ditem module, 19 p.

Hay, J.E., 1979. Calculation of monthly mean solar radiation for horizontal and inclined surfaces. *Solar Energy*, Vol. 23, pp. 301-307.

Hay, J.E., and D.C. McKay, 1985. Estimating solar irradiance on inclined surfaces: A review and assessment of methodologies. *Int. J. Solar Energy*, Vol. 3, pp. 203-240.

Hay, J.E., R. Perez, and D.C. McKay, 1986. Addendum and errata to the paper estimating solar irradiance on inclined surfaces: A review and assessment of methodologies. *Int. J. Solar Energy*, Vol. 4, pp. 321-324.

Holben, B.N., and C.O. Justice, 1981. An examination of spectral band ratioing to reduce the topographic effect of remotely sensed data. *International Journal of Remote Sensing*, Vol. 2, pp. 115-123.

Horler, D.N.H., and F.J. Ahern, 1986. Forestry information content of Thematic Mapper Data. *International Journal of Remote Sensing*, Vol. 7, pp. 405-428.

Hudson, W.D., and C.W. Ramm, 1987. Correct formulation of the Kappa coefficient of agreement. *Photogrammetric Engineering & Remote Sensing*, Vol. 53, No. 4, pp. 421-422.

Iqbal, M., 1983. *An introduction to Solar Radiation*, Academic Press, New York.

Kaufman, Y.J., 1989. The atmospheric effect on remote sensing and its corrections. *Theory and Applications of Optical Remote Sensing* (G. Asrar, editor), John Wiley & Sons, New York, pp. 336-428.

Liou, K.N., 1980. *An Introduction to Atmospheric Radiation, Academic Press*, New York.

Maselli, F., C. Conese, L. Petkov, and R. Resti, 1992. Inclusion of prior probabilities derived from a nonparametric process into the maximum-likelihood classifier. *Photogrammetric Engineering & Remote Sensing*, Vol. 58, pp. 201-207.

Naugle, B.I., and J.D. Lashlee, 1992. Alleviating topographic influences on land-cover classifications for mobility and combat modeling. *Photogrammetric Engineering & Remote Sensing*, Vol. 58, No. 8, pp. 1217-1221.

Pouch, G.W., and D.J. Campagna, 1990. Hyperspherical direction cosine transformation for separation of spectral and illumination information in digital scanner data. *Photogrammetric Engineering & Remote Sensing*, Vol. 56, No. 4, pp. 475-479.

Price, J.C., 1987. Calibration of satellite radiometers and the comparison of vegetation indices. *Remote Sensing of Environment*, Vol. 21, pp. 15-27.

Proy, C., D. Tanr, and P.Y. Deschamps, 1989. Evaluation of topographic effects in remotely sensed data. *Remote Sensing of Environment*, Vol. 30, pp. 21-32.

Saunders, R.W., 1990. The determination of broad band surface albedo from AVHRR visible and near-infrared radiances, *International Journal of Remote Sensing*, Vol. 11, No. 1, pp. 49-67.

Sturm, B., 1981. The atmospheric correction of remotely sensed data and the quantitative determination of suspended matter in marine water surface layers. *Remote Sensing in Meteorology, Oceanography and Hydrology* (A.P. Cracknell, editor), Ellis Horwood Limited, England, chapter 11.

Temps, R.C., and K.L. Coulson, 1977. Solar radiation incident upon slopes of different orientations. *Solar Energy*, Vol. 19, pp. 179-184.

Utrillas, M.P., J.A. Martinez-Lozano, and A.J. Casanovas, 1991. Evaluation of models for estimating solar irradiation on vertical surfaces at Valencia, Spain. *Solar Energy*, Vol. 47, No. 3, pp.223-229.

Zibordi, G., and G. Maracci, 1988. Determination of atmospheric turbidity from remotely-sensed data. A case study. *International Journal of Remote Sensing*, Vol. 9, No. 12, pp. 1881-1894.

(Received 11 August 1992; revised and accepted 14 January 1993)

LIST OF "LOST" CERTIFIED PHOTOGRAMMETRISTS

We no longer have valid addresses for the following Certified Photogrammetrists. If you know the whereabouts of any of the persons on this list, please contact ASPRS headquarters so we can update their records and keep them informed of all the changes in the Certification Program. Thank you.

Jack R. Anthony	Robert Fuoco	F.A. Hildebrand, Jr.	Harry J. Miller	Keith Syrett
Dewayne Blackburn	Franek Gajdeczka	James Hogan	Marinus Moojen	William Thomasset
Gerard Borsje	George Glaser	William Janssen	M. David L. Morgan	Conrad Toledo
Eugene Caudell	William Grehn, Jr.	Lawrence Johnson	Gene A. Pearl	Robert Tracy
Robert Denny	Louis T. Harrod	Spero Kapelas	Sherman Rosen	Lawrence Watson
		Andre J. Langevin	Lane Schultz	Tad Wojenka